Preequilibrium (p,p') spectra for nuclei around neutron number 50

Y. Watanabe, I. Kumabe, M. Hyakutake,* N. Koori, K. Ogawa,† K. Orito,† K. Akagi,† and N. Oda‡

Department of Nuclear Engineering, Kyushu University, Fukuoka 812, Japan

(Received 22 May 1987)

Energy spectra of protons emitted from (p,p') scattering were measured for ^{90}Zr, ^{93}Nb, ^{92,94,96,98,100}Mo, ^{106}Pd, and Ag at an incident energy of 18 MeV. It was shown that there were no appreciable shell and odd-even effects on the preequilibrium proton spectra corresponding to excitations higher than 4 MeV of the residual nucleus. The experimental results were interpreted on the basis of the state densities generated from two sets of single particle levels using the recursion method by Williams *et al.*; one is based on the spherical Nilsson model, and the other on the modified uniform spacing model in which a shell gap is introduced into the uniform spacing model. The measured angle-integrated proton spectra were compared with those calculated on the basis of the exciton model and the Hauser-Feshbach model in which the isospin selection rule was taken into account. Good agreement between the experimental and calculated spectra was obtained for all targets in the continuum region in the outgoing proton energy region of 3–14 MeV.

I. INTRODUCTION

Recently, Scobel *et al.*[1] have performed systematic measurements of neutron spectra emitted from 18 and 25 MeV (p,n) reactions with nuclei near neutron number 50 in order to investigate the shell effect in the preequilibrium process. Moreover, Mordhorst *et al.*[2] have reported a study of the odd-even effect due to pairing correlations on preequilibrium spectra of emitted neutrons from 25.6 MeV (p,n) reactions with Mo isotopes. As predicted in earlier works by Williams *et al.*[3] and Albrecht and Blann,[4] pronounced structures due to a shell gap at the shell closure and the grouping of single particle levels were observed in the high energy portion of (p,n) spectra for the nuclei near shell closure measured by both groups.[1,2] These structures were interpreted in terms of $(p)(n)^{-1}$ state densities generated from different sets of realistic single particle schemes.

Inelastic scattering is a major reaction channel in reactions induced by several tens of MeV nucleon. It preferentially excites $(n)(n)^{-1}$ or $(p)(p)^{-1}$ states; the (p,n) reactions mainly populate $(p)(n)^{-1}$ states. Studies of inelastic scattering will provide an effective method with which to investigate the shell and odd-even effects on the density of particle-hole states in the same shell [e.g., $(n)(n)^{-1}$ or $(p)(p)^{-1}$ states]. For nucleon inelastic scattering, however, systematic measurements of continuum spectra of the emitted nucleons have not so far been carried out in order to study the shell and odd-even effects in the preequilibrium process, in contrast to the (p,n) reactions.[1,2,5,6]

In the present work, therefore, we have measured systematically the energy spectra of protons emitted from 18 MeV (p,p') scattering by targets chosen as follows: shell closed nuclei with neutron number 50 (^{90}Zr and ^{92}Mo), nuclei near the shell closure (^{93}Nb and ^{94,96,98,100}Mo), and a pair of even-even and odd nuclei which are far from the shell closure (^{106}Pd and natural Ag).

In the inelastic scattering, strong peaks corresponding to collective excitations due to direct processes (e.g., 2^+ and 3^- levels for the even-even nuclei) are observed in the low excitation region of the (p,p') spectra. The preequilibrium model cannot account for the direct excitation of these collective levels, which involve the correlated motion of many particles. Accordingly, we focus attention on the continuum region corresponding to residual excitations above 4 MeV of the measured (p,p') spectra; in the region, influences of collective excitations are expected to become relatively small. The aim of the present work is to see how the shell and odd-even effects will appear in the continuum proton spectra, and to interpret the experimental results in terms of realistic partial state density within the framework of the preequilibrium model.

II. EXPERIMENTAL PROCEDURE

A. Measurement

The experiment was performed using an 18 MeV proton beam from the tandem Van de Graaff accelerator at Kyushu University. The experimental procedure has been described in detail elsewhere.[7] Emitted protons were detected with a silicon ΔE-E counter telescope consisting of a 75 μm surface barrier detector and a 2500 μm Li-drifted detector. A defining aperture of 6 mm diameter was placed just in front of the ΔE detector and was located 178 mm from the target. Signals of protons were separated from those of other charged particles with a particle identification circuit. Pulse height spectra were measured at intervals of 10° from 30° to 160°.

The beam intensity was determined with a current integrator connected to a Faraday cup and was also monitored by a detector located at a fixed backward angle to the beam. Targets were self-supporting metallic foils, 0.5–1 mg/cm^2 thick. Detailed information on the targets is listed in Table I of Ref. 7.

B. Data processing

The measured pulse height spectra were converted to energy spectra and angular distributions in the c.m. system. Two kinds of backgrounds were carefully subtracted in the data processing. One is the continuous background due to the slit scattering of elastic protons by the detector aperture. It was estimated under the assumption that the 30° spectrum measured using a gold target could be attributed to the degraded elastic protons. The 30° spectrum for gold was subtracted from the other measured spectra after normalizing the counts of elastic peaks. The correction amounted to about 60% at 30°, but decreased rapidly with increasing angle and became less than 1% at backward angles.

The other component of background consisted of discrete peaks due to light-element impurities on the targets, such as hydrogen, carbon, and oxygen. After these peaks were identified in the measured spectra, they were subtracted by drawing a curve under the peak on the assumption that the spectrum must be smooth in the continuum region.

Absolute cross sections were determined by normalizing the experimental elastic cross sections to the optical model predictions at forward angles, because the errors arise from the nonuniformity of target thickness. The normalization factors for two sets of global optical model parameters[8,9] were compared in order to estimate the uncertainties involved in this method. Consequently, the uncertainty associated with the normalization was estimated to be within 10% for each target. However, the relative uncertainty of the cross sections for different targets is believed to be less than 4%. Finally, the normalization factors obtained from the optical model parameter of Becchetti and Greenlees[8] were adopted.

To obtain an angle-integrated spectrum, the experimental angular distributions for each 0.2 MeV energy bin were fitted with a series of Legendre polynomials up to $l=4$, and then the polynomials were integrated.

III. EXPERIMENTAL RESULTS

Energy spectra of protons emitted from ^{93}Nb(p,xp) reaction are illustrated for several angles in Fig. 1. The angular distributions are peaked forward in the continuum region between 6 and 14 MeV. This suggests that the preequilibrium process is dominant in this region. The measured proton spectra for the other targets also have similar continuum regions to that shown in Fig. 1.

The angle-integrated spectra of protons emitted from (p,xp) reactions are shown for ^{90}Zr, ^{93}Nb, ^{92,94,96,98,100}Mo, ^{106}Pd, and Ag in Fig. 2. The spectra for the outgoing energies higher than 14 MeV were excluded from analyses by the preequilibrium model, because they show pronounced structures corresponding to the excitation of collective levels, such as the lowest 2^+ and 3^- levels of even-even nuclei. The spectra for ^{90}Zr, ^{92}Mo, and ^{94}Mo indicate relatively strong evaporation peaks at low energies of emitted protons; particularly, contributions of protons from (p,np) and/or (p,2p) processes are large in the outgoing energy region below 6 MeV for ^{90}Zr and below 5 MeV for ^{92}Mo. The proton spectra for shell closed nuclei (^{90}Zr and ^{92}Mo) with neutron number 50 have noticeable structures in outgoing energies above 10 MeV. These structures may be related to a large energy gap that exists at the magic number in the neutron shell. For nuclei away from the shell closure, the spectra exhibit trends to be flat and smooth with increasing neutron number, and they have a similar shape and almost the same magnitude within several percent in the continuum region above 10 MeV. However, the cross sections for ^{92}Mo and ^{94}Mo are larger than those for the other targets in the outgoing energies between 10 and 14 MeV, because the equilibrium components for ^{92}Mo and

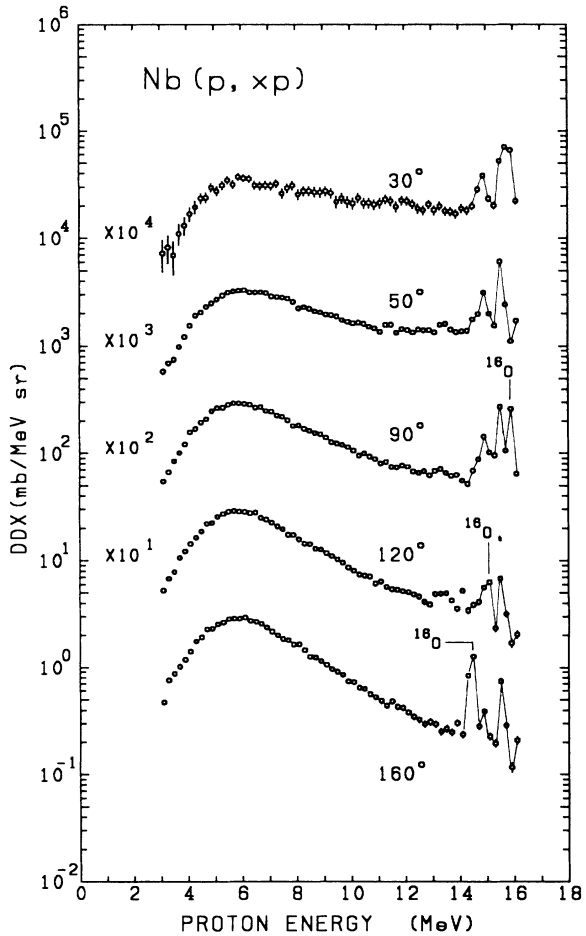

FIG. 1. Double differential cross sections for the ^{93}Nb(p,xp) reaction at the bombarding energy of 18 MeV. Angles represented are in the laboratory system. Energies are in the center of mass system. The peaks labeled ^{16}O correspond to elastic scattering on an impurity ^{16}O.

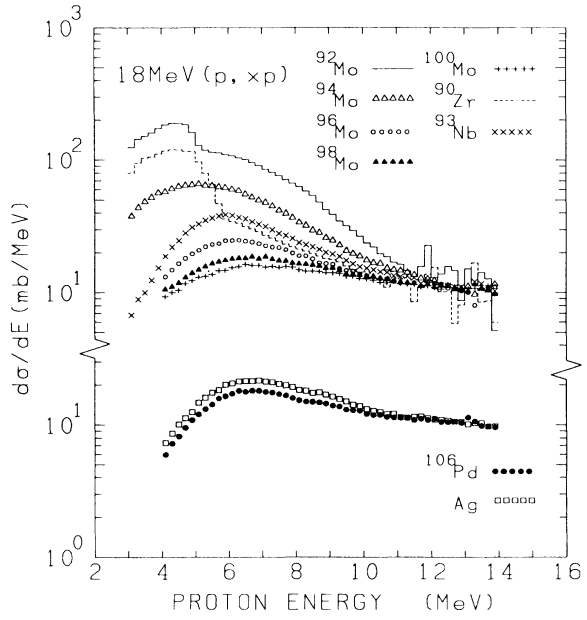

FIG. 2. Angle-integrated energy spectra of protons emitted from the (p,xp) reaction on ^{90}Zr, ^{93}Nb, ^{92,94,96,98,100}Mo, ^{106}Pd, and Ag at the bombarding energy of 18 MeV.

^{94}Mo are larger than that for the others. The equilibrium component, therefore, should be subtracted from the experimental data in the energy region of interest in order to estimate contributions from the preequilibrium process.

In Fig. 3 we present nonequilibrium cross sections integrated over 10–13 MeV after subtraction of the equilibrium component. The equilibrium cross sections were estimated in two ways. One is the calculated cross section using the Hauser-Feshbach model described in Sec. IV C. The other is the measured cross section at a backward angle $\theta = 160°$ that was assumed to correspond to the equilibrium component with an isotropic angular distribution. Parts (a) and (b) in Fig. 3 show the results (σ_a and σ_b) for subtraction of the equilibrium components obtained in the above two ways, respectively. An error associated with the subtraction was estimated to be 5% for all the target isotopes; the relative uncertainty between different targets is also included in the error. Although the absolute values of the nonequilibrium cross sections σ_a and σ_b are different, each is nearly equal between the measured isotopes within the error. One of the reasons for different absolute values is that the way to derive σ_b probably overestimates the equilibrium component because nonequilibrium components are included with some fractions even at backward angles.

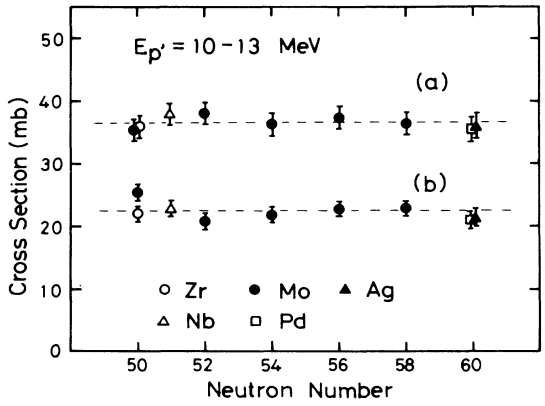

FIG. 3. Nonequilibrium cross sections integrated over 10–13 MeV after subtraction of equilibrium component. See text for details of subtraction methods for (a) and (b). Dashed horizontal lines denote the averaged nonequilibrium cross section.

Studies of inelastic proton scattering at the incident energy of near 18 MeV on Sn isotopes have been reported in earlier works by Cohen *et al.*[10] and Kalbach *et al.*;[11] isotopes of Sn are nuclei far from the neutron shell closure. The measured energy spectra have similar shape and nearly equal magnitude in the excitation energy region 4–8 MeV, except the spectrum for ^{112}Sn, which has a large equilibrium component. This trend is the same as that for Mo isotopes measured in the present work. Consequently, the experimental results for both Mo isotopes and Sn isotopes indicate that there is no appreciable shell effect on the preequilibrium (p,p') spectra corresponding to excitations higher than 4 MeV.

Furthermore, the odd-even effect on the preequilibrium process can be investigated by comparing experimental results of the odd and even-even nucleus pairs of ^{93}Nb-^{94}Mo and Ag-^{106}Pd. Although the proton spectra for ^{93}Nb and ^{94}Mo are different in shape and magnitude in the whole energy region, this is attributable to different contributions from the equilibrium process. Subtraction of the equilibrium component from the experimental data yields almost the same cross section for both spectra, as shown in Fig. 3. The proton spectra for Ag and ^{106}Pd have the same magnitude and shape above 10 MeV in Fig. 2. The odd-even effect, therefore, does not obviously appear in the preequilibrium (p,p') spectra corresponding to excitations above 4 MeV for target nuclei near shell closure as well as those away from shell closure.

IV. THEORETICAL ANALYSES AND DISCUSSIONS

A. The closed form expression of the exciton model

In terms of the closed form expression of the exciton model,[12,13] the energy spectra of the emitted particle from nucleon induced reactions can be represented as follows,

$$\frac{d\sigma_x}{d\epsilon} = \sigma_{\text{abs}} \sum_{\substack{n=n_0 \\ \Delta n=+2}}^{\bar{n}} \frac{W_x(n,\epsilon)}{\lambda_{n\to n+2} + W_n} D_n \ , \tag{1}$$

where D_n is the depletion factor given by

$$D_n = \prod_{i=n_0}^{n-2} \frac{\lambda_{i\to i+2}}{\lambda_{i\to i+2}+W_i} , \tag{2}$$

and $\sigma_{\rm abs}$ is the composite nucleus formation cross section. The quantity $W_x(n,\epsilon)$ denotes the emission rate of a particle of type x with energy ϵ from the n exciton state and is given by

$$W_x(n,\epsilon)d\epsilon = \frac{2s_x+1}{\pi^2\hbar^3}\mu_x \epsilon \sigma_{x,\rm inv}(\epsilon)\frac{\omega_{\rm p-1,h}(U)}{\omega_{\rm p,h}(E)}Q_x({\rm p})d\epsilon , \tag{3}$$

where s_x is the spin of emitted particle of type x, μ_x the reduced mass, $\sigma_{x,\rm inv}(\epsilon)$ the inverse reaction cross section, and $Q_x({\rm p})$ the correction factor for the distinguishability of proton and neutron degrees of freedom.[14] The quantity ω_n denotes the partial state density with the exciton configuration n at the excitation energy E (or U) of the composite (or residual) nucleus. On the basis of the Fermi gas model with uniform spacing g^{-1}, we have[15]

$$\omega_{\rm p,h}(E) = \frac{g(gE-A({\rm p,h}))^{n-1}}{{\rm p!h!}(n-1)!} \tag{4}$$

for the exciton configuration n with the number of particle p and hole h. The correction term $A({\rm p,h})$ is due to the Pauli exclusion principle.

The quantity W_n in Eq. (1) or W_i in Eq. (2) is calculated by integration of $W_x(n,\epsilon)$ as follows,

$$W_{n\ ({\rm or}\ i)} = \sum_x \int_0^{E-B_x} W_x(n,\epsilon)d\epsilon , \tag{5}$$

where B_x is the binding energy of a particle of type x. The transition rate from the n exciton state to the $n+2$ exciton state $\lambda_{n\to n+2}$ in Eq. (1) [or $\lambda_{i\to i+2}$ in Eq. (2)] is calculated from[16]

$$\lambda_{n\to n+2} = \frac{2\pi}{\hbar}|M|^2 \frac{g}{2(n+1)} \frac{[gE-A({\rm p+1,\ h+1})]^{n+1}}{[gE-A({\rm p,h})]^{n-1}} , \tag{6}$$

where $|M|^2$ is the squared average transition matrix element.

B. Microscopic calculation of partial state density

Preliminary results of the exciton model calculation [Eq. (1)] have shown that the fraction of $n=n_0=3$ becomes about 80% in the proton energy region 10–14 MeV. The term of $n=3$ in Eq. (1) is reduced to an approximate relation given by

$$\left[\frac{d\sigma_x}{d\epsilon}\right]_{n=3} \propto \epsilon\sigma_{x,\rm inv}(\epsilon)\omega_{1,1}(U) . \tag{7}$$

It should be noted that the inverse reaction cross section $\sigma_{x,\rm inv}(\epsilon)$, which is calculated using the optical model, is a smooth function of mass number and atomic number. In order to interpret disappearance of the shell and odd-even effects in the preequilibrium proton spectra, therefore, we should investigate quantitatively the effect of nuclear shell structure and pairing interaction on the p-h state density $\omega_{\rm p,h}(U)$.

The p-h state density given by Eq. (4) is widely used in the preequilibrium model calculation. This formula is derived from single particle levels of an equidistant spacing as shown in Fig. 4(c). On the other hand, as shown in Fig. 4(a), a large gap (3–4 MeV) and groupings of levels appear in the realistic single particle level scheme based on the spherical Nilsson model.[17] If the state density $\omega_{\rm p,h}(U)$ is derived from such single particle levels, the effect of shell gap and level grouping can be introduced.

Scobel *et al.*[1] have calculated $({\rm p})({\rm n})^{-1}$ state densities from different sets of realistic single particle levels using the recursion method given by Williams[3] and have explained structures that appear in the low excitation region of the (p,n) spectra. Similarly, we performed microscopic calculations of $({\rm n})({\rm n})^{-1}$ and $({\rm n})^2({\rm n})^{-2}$ state densities for Mo isotopes on the basis of the spherical Nilsson model. Pairing correlation was taken into account under the quasiparticle approximation. Then, the two quasiparticle excitation energy is given by[18]

$$E_{j,j'} = [(\epsilon_j-\lambda)^2+\Delta^2]^{1/2}+[(\epsilon_{j'}-\lambda)^2+\Delta^2]^{1/2} , \tag{8}$$

where subscripts j and j' represent orbits below and above the Fermi energy λ, respectively, ϵ the single particle energy, and Δ the pairing energy, which was taken

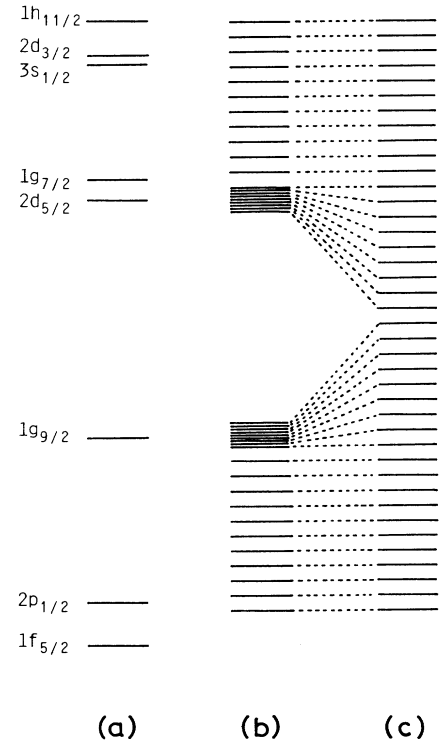

FIG. 4. Single particle level schemes for neutron shell: (a) spherical Nilsson model, (b) modified uniform spacing model, and (c) uniform spacing model.

to be equal to $12A^{-1/2}$ from odd-even mass differences.[19] In order to explain, roughly, the spreading of the single particle strengths due to the residual interaction, the calculated partial state densities were smoothed using a Gaussian distribution function of 1.0 MeV width.

In Fig. 5 we present the results obtained for ^{92}Mo, ^{96}Mo, and ^{100}Mo using solid curves. Dotted curves indicate the $(n)(n)^{-1}$ state density generated from the equidistant spacing level modified so as to have a wide shell gap at the shell closure, as shown in Fig. 4(b); this model will be referred to as the modified uniform spacing (MUS) model.[7,20] The spacing between levels was taken to be equal to $13/N$ (in MeV), where N is the neutron number. The energy gap was chosen to be that derived from the Nilsson model.[17] Note that the $(n)(n)^{-1}$ state densities for ^{96,100}Mo have small values in excitations less than 2Δ in Fig. 5, because of smoothing with a Gaussian function of 1.0 MeV width.

We will summarize noteworthy points for the obtained p-h state densities. In the case of ^{92}Mo in Fig. 5(a), the influence of the shell gap appears in the low excitation region; there is no $(n)(n)^{-1}$ state in the region. The density of $(n)(n)^{-1}$ states exhibits a steep rise around 4 MeV and structures with broad peaks due to the grouping of single particle levels up to about 15 MeV. As excitation energy increases, the $(n)(n)^{-1}$ state density obtained from the MUS model can successfully explain the averaged behavior of that from the Nilsson model.

In the cases of ^{96}Mo and ^{100}Mo, the addition of several neutrons above the $N=50$ shell closure moderates the effect of shell gap on the $(n)(n)^{-1}$ state density as shown in Figs. 5(b) and (c). Fluctuations indicated in low excitations become smaller than those for ^{92}Mo. Consequently, the $(n)(n)^{-1}$ state density based on the MUS model reproduces well the overall behavior of that based on the Nilsson model in excitation energies above 5 MeV. Furthermore, for ^{100}Mo in a new deformed region as noted in Ref. 2, if we take into account the nuclear deformation in the Nilsson model, single particle levels would approach to the equidistant levels owing to splits of a single particle level (j) into levels of $(2j+1)/2$. Thus much less structure is expected for the resultant $(n)(n)^{-1}$ state density and it would become as smooth as the $(n)(n)^{-1}$ state density from the MUS model.

On the basis of the derived $(n)(n)^{-1}$ state density, we will discuss no pronounced shell effect for nuclei near the shell closure that has been observed on the measured spectra in the excitation energy region above 4 MeV. In such excitations the influence of a shell gap on the calculated $(n)(n)^{-1}$ state densities is significantly reduced for all three isotopes. Moreover, they have the trend of increasing monotonically with neutron excess. Hence, an appreciable shell effect is not found in the observed continuum (p,p') spectra corresponding to intermediate excitations of above 4 MeV.

Furthermore, in order to see the contribution of the emission from $n=5$ states we also have calculated the state densities of the $(n)^2(n)^{-2}$ configuration, one of the $n=4$ configurations of the residual nucleus, on the basis of the Nilsson model. The results are shown by dashed curves in Fig. 5. The $(n)^2(n)^{-2}$ state density for ^{92}Mo is quite different from that for ^{96}Mo or ^{100}Mo, especially in excitation energies of 5–10 MeV. This implies that the effect of the shell gap can be enhanced with an increase in exciton number if there is no residual interaction. However, this effect may not be dominant in the proton energy spectra, because the contribution of $n \geqq 5$ is estimated to be only about 20% and the other configurations [e.g., the $(n)(n)^{-1}(p)(p)^{-1}$ and $(p)^2(p)^{-2}$ configurations] are also responsible for the $n=4$ states of the residual nucleus.

The (p,n) spectra measured by Scobel *et al.*[1] and Mordhorst *et al.*[2] have a structureless continuum in outgoing neutron energies below 18 MeV, except for isobaric-analog-state (IAS) peaks and small peaks corresponding to the transitions to low lying states for ^{90}Zr and ^{92}Mo. The shape and magnitude of the spectra in this energy region change smoothly with increasing neutron number. Therefore, these observations indicate that

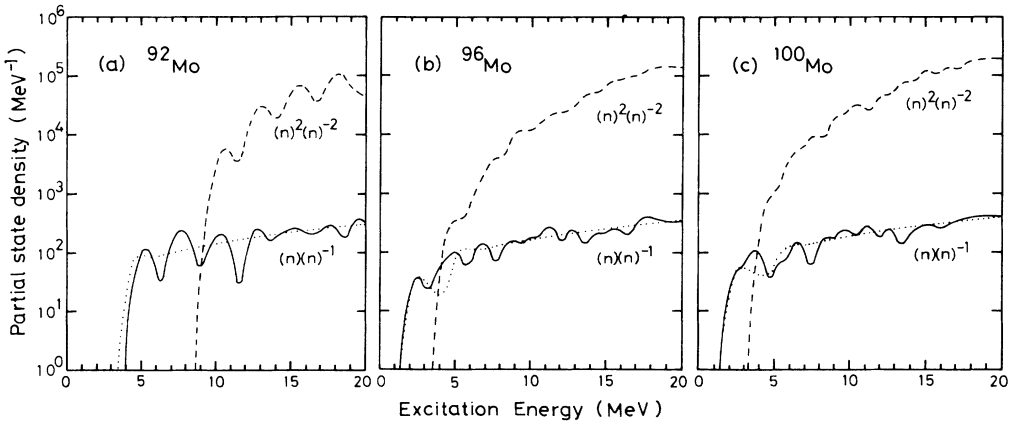

FIG. 5. Partial state densities for 1p-1h neutron configurations $[(n)(n)^{-1}]$ and 2p-2h neutron ones $[(n)^2(n)^{-2}]$ for ^{92,96,100}Mo. Solid and dashed curves represent state densities generated using the spherical Nilsson model. Dotted curves are the results of the modified uniform spacing model.

there is no appreciable shell effect in the (p,n) spectra as well as in the (p,xp) spectra measured in the present work, when the discussion is limited to the intermediate excitation region of more than 4 MeV. Similar trends were also observed in 18 MeV (p,α) spectra for Mo isotopes measured by some of the authors.[7] Detailed discussion based on the MUS model is reported for the (p,n) spectra and the (p,α) spectra elsewhere.[7,20]

The microscopic calculation of $(p)(p)^{-1}$ state density has been performed for an odd- and even-A pair of ^{107}Ag and ^{106}Pd in order to investigate no appreciable odd-even effect on the measured proton spectra. The results from the spherical Nilsson model are shown by solid curves in Fig. 6. Dotted curves are the densities derived from the uniform spacing (US) model, in which the equidistant spacing was chosen to be $13/Z$, where Z is the atomic number, and pairing correlation was introduced using Eq. (8). In the case of ^{107}Ag, the $(p)(p)^{-1}$ states due to the excitation of an unpaired proton appear at excitation energies below 2 MeV. On the other hand, the density of $(p)(p)^{-1}$ states for ^{107}Ag is almost identical with that of ^{106}Pd in the excitation energy region above 2 MeV, because excitations of broken proton pairs are dominant. The state densities of the $(p)(p)^{-1}(n)(n)^{-1}$ configuration were also compared between ^{106}Pd and ^{107}Ag as shown by dashed curves in Fig. 6. Both of the state densities become equal as the excitation energy increases, although obvious differences exist only in low excitation energies. Thus, from consideration about the state density it can be understood that the measured (p,p′) spectra for ^{106}Pd and Ag coincide nearly in shape as well as in magnitude in the outgoing proton energies of 10–14 MeV. Furthermore, the fraction of proton configuration $(p)(p)^{-1}$ included in total 1p-1h state density is expected to be smaller than that of the neutron configuration $(n)(n)^{-1}$, because the interaction between like nucleons is weaker than that between unlike nucleons.[21] This may, therefore, give another reason for no odd-even effect on the preequilibrium (p,p′) spectra.

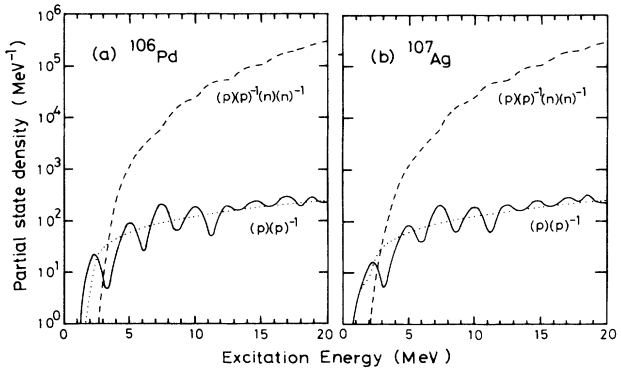

FIG. 6. Partial state densities for 1p-1h proton configurations $[(p)(p)^{-1}]$ and one proton particle–one proton hole and one neutron particle–one neutron hole configurations $[(p)(p)^{-1}(n)(n)^{-1}]$ for ^{106}Pd and ^{107}Ag. Solid and dashed curves represent state densities generated using the spherical Nilsson model. Dotted curves are the results of the uniform spacing model.

Upon comparison with $d\sigma/d\epsilon$ at given excitation energies U, Mordhorst *et al.*[2] have reported a pronounced odd-even effect in the (p,n) spectra for Mo isotopes. If we compare them at given outgoing neutron energies ϵ_n, however, the continuous part of the spectra show a smooth change in magnitude for $^{92-100}$Mo in which odd-A and even-even nuclei are included.[20] The difference between two interpretations for (p,n) reactions can be explained according to Eq. (7) as follows. For the odd target nucleus, low lying states ($U<2\Delta$) of the residual nucleus are excited by emission of an unpaired neutron, and high lying states ($U>2\Delta$) are mainly due to emission of one of paired neutrons. The relative contribution of an unpaired neutron becomes small with increasing excitation energy. For an even-even target nucleus, all residual excited states ($U>0$) are formed by emissions of one of the paired neutrons. Therefore, $\omega_{1,1}(U-2\Delta)$ for the odd target nucleus is almost equivalent to $\omega_{1,1}(U)$ for the neighboring even-even target nucleus. On the other hand, the energy difference between the ground state Q value for the odd-A and even-even nuclei is nearly equal to 2Δ, and the neutron inverse cross section $\sigma_{n,inv}(\epsilon)$ is approximately constant in the neutron energy region under consideration. Thus, no odd-even effect is appreciably observed in $d\sigma/d\epsilon$ versus outgoing neutron energies ϵ_n, except for the low excitation energy region.

C. Proton energy spectra: Calculations and comparison

We calculated angle-integrated (p,xp) spectra for the measured nuclei in terms of the exciton model (Sec. III A) and the Hauser-Feshbach model.[22] The calculated spectra were compared with the measured ones in Figs. 7 and 8.

Since the isospin conservation rule plays an important role in proton emissions in the proton induced reaction,[11,23] we introduced isospin as a quantum number in the closed-form expression under the two following assumptions.

(i) The damping of fluxes from higher isospin $T_>$ states to lower isospin $T_<$ states is completely neglected in preequilibrium process; namely, this is an assumption of no mixing between $T_>$ and $T_<$ states.

(ii) Only neutron and proton emissions compete in the preequilibrium process, because the possibility of α-particle emissions is smaller than that of nucleon emissions.

As a result, preequilibrium emissions from two different isospin states in the composite nucleus were treated independently according to Eq. (1). Isospin weighting factors determined by the Clebsch-Gordon coefficient for the isospin coupling were used to obtain the cross sections for the formation of $T_<$ and $T_>$ composite states and the proton inverse cross sections for each composite state decay. The parameters employed in the calculations are summarized in Table I. The densities of the $T_<$ and $T_>$ isospin states are given by

$$\omega^{<}_{p,h}(E)=\omega_{p,h}(E)\ , \tag{9a}$$

$$\omega^{>}_{p,h}(E)=\omega_{p,h}(E-E_{sym})\ , \tag{9b}$$

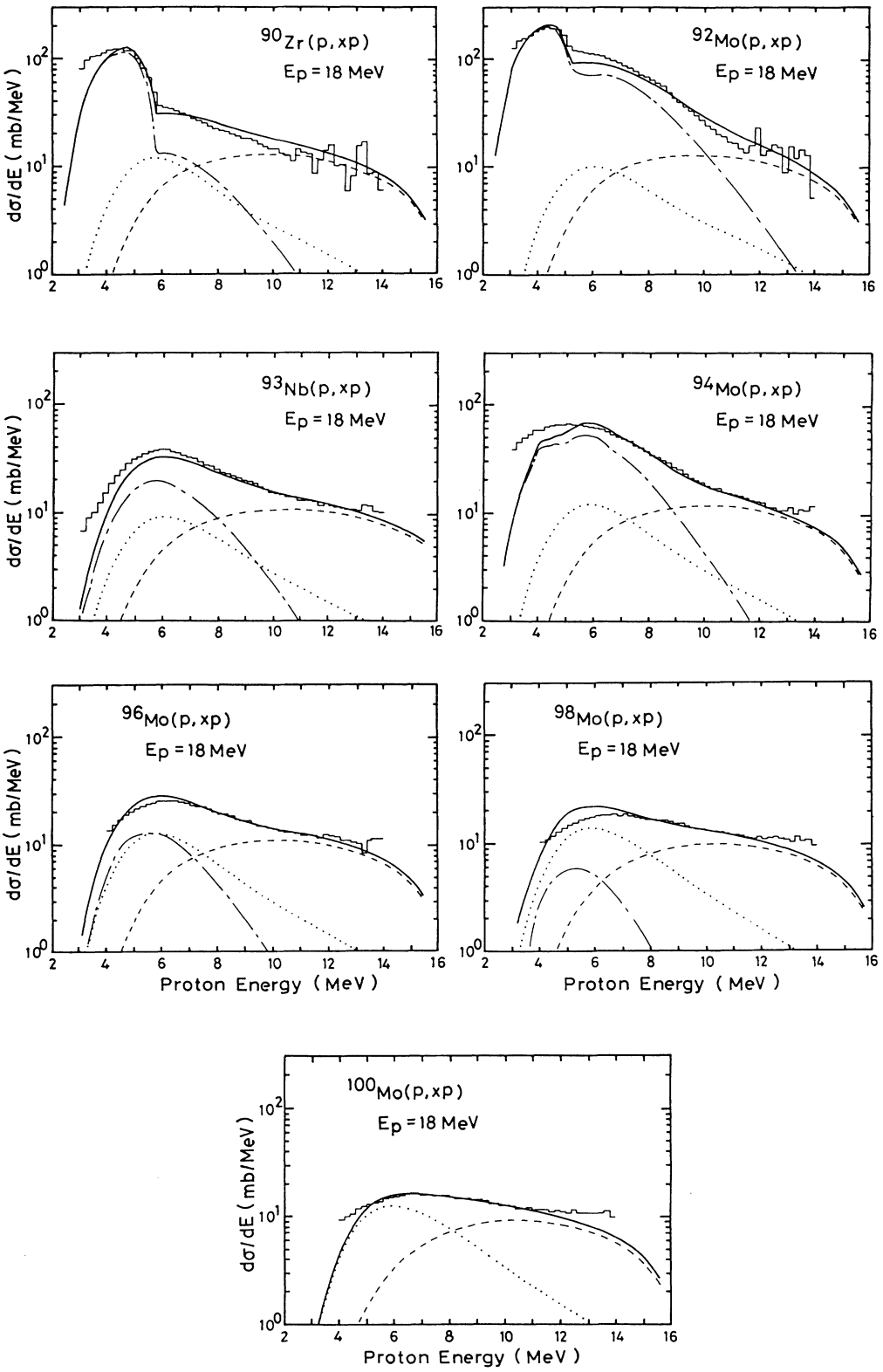

FIG. 7. Calculated and experimental (p,xp) spectra for ^{90}Zr, ^{93}Nb, and ^{92,94,96,98,100}Mo. Histgrams represent the experimental angle-integrated spectra. Solid curves are the total calculated energy spectra. Dashed curves are the $T_<$ component of the calculated preequilibrium energy spectra using the exciton model; dotted curves are the $T_>$ component of the same. Dashed-dotted curves show the calculated equilibrium spectra using the Hauser-Feshbach model. A dashed-dotted curve for ^{100}Mo is not illustrated because the calculated equilibrium spectrum was very small.

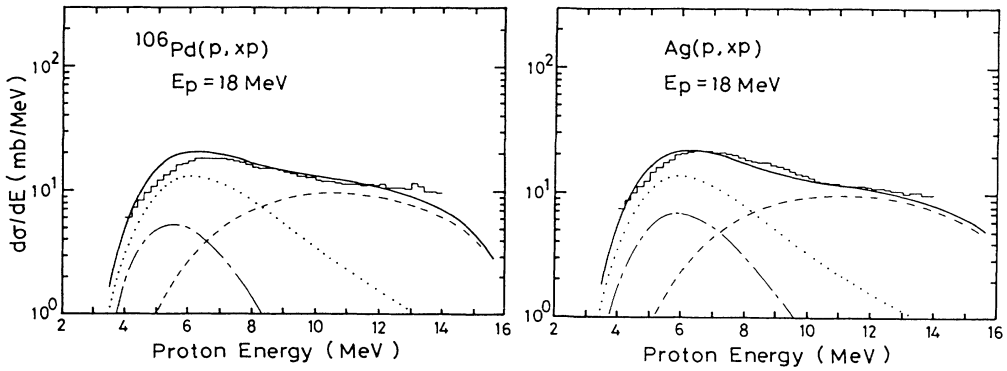

FIG. 8. Calculated and experimental (p,xp) spectra for ^{106}Pd and Ag. See also the caption of Fig. 7.

where E_{sym} is the nuclear symmetry energy.[29] As the p-h state density Eq. (4), with a shell-independent parameter $g = A/13$, was used because the MUS and US models were found to reproduce successfully the average property of the 1p-1h state density based on the Nilsson model in the excitation energy region above 4 MeV, as shown in Figs. 5 and 6. The standard pairing shift Δ proposed by Blann *et al.*[27] was employed as the pairing correction for the state density of composite and residual nuclei. The quantities g and Δ for the analog system were chosen for $T_>$ composite states. The same $|M|^2$ was used for both isospin states. The parameter K value[28] was determined so as to reproduce well the spectra for nuclei away from the shell closure (i.e., ^{106}Pd and Ag in Fig. 8).

Next, the Hauser-Feshbach formalism,[24] taking the isospin into account, was employed in the calculation for the equilibrium process. We assumed that complete mixing occurs when equilibrium is reached, and the fluxes of $T_>$ states after preequilibrium decay fully damp into $T_<$ states. This means that $\mu = 1$ in Eq. (3.5) in Ref. 24. The competition of neutron, proton, α-particle, and γ-ray emissions, and multiparticle emission processes, were considered in the present calculation of the equilibrium cross sections. The parameters used in the calculation are listed in Table I. Level density parameters a for several nuclei have been adjusted within a few percent so as to reproduce successfully the experimental spectra for ^{90}Zr, ^{92}Mo, ^{94}Mo, and ^{93}Nb. Moreover, the γ-decay width calculated from the Brink-Axel form[31,32] was normalized to the empirical formula given by Malekey *et al.*[36]

The calculated spectra agree well with the experimental ones for all of the target nuclei, except for two shell

TABLE I. Input parameters used in the exciton model and Hauser-Feshbach model calculations.

Input parameter	Input parameter source: Exciton model	Input parameter source: Hauser-Feshbach Model
Transmission coefficient (reaction and inverse cross section)	n: Wilmore and Hodgson[a] p: Mani *et al.*[b]	n: Wilmore and Hodgson[a] p: Mani *et al.*[b] α: Huizenga and Igo[c] γ: Brink-Axel giant dipole resonance form for $E1$ transition[d] Weisskopf form for $M1$ and $E2$ transition[e]
Level density		Gilbert and Cameron[f] Discrete levels for low lying excitations[g]
Single particle level density parameter	$g = A/13$	
Pairing correction	Standard pairing shift[h]	
K value[i] ($\|M\|^2 = KA^{-3}E^{-1}$)	430 MeV[3]	
Symmetry energy	J. D. Anderson *et al.*[j]	

[a]Reference 25.
[b]Reference 26.
[c]Reference 30.
[d]References 31 and 32.
[e]Reference 33.
[f]Reference 34.
[g]Reference 35.
[h]Reference 27.
[i]Reference 28.
[j]Reference 29.

closed nuclei ^{90}Zr and ^{92}Mo in the energy region where the preequilibrium process is dominant. In the proton energy region of 10–14 MeV, overestimations for ^{90}Zr and ^{92}Mo(p,xp) spectra may be due to the effect of the shell gap on 2p-2h state densities, because this effect was predicted to be small but not negligible for shell closed nuclei, as mentioned in Sec. III B.

As shown in Figs.7 and 8, the $T_>$ component is responsible for the low energy part of the calculated preequilibrium spectra, and the $T_<$ component holds the high energy part. This trend is similar to the results of Kalbach *et al.*, who have calculated the (p,p') spectra for Sn isotopes using the master equation approach[11]. In the proton energy region of 10–14 MeV, contribution of the $T_>$ component was only about 15% in the preequilibrium cross sections for all the targets. This figure may indicate an upper limit obtained under the assumptions of no mixing between $T_>$ and $T_<$ states. Therefore, the isospin effect is not enough to explain the disappearance of the shell effect in the preequilibrium (p,p') spectra, although it is important for proton emissions in proton induced reactions.

The preequilibrium emission from $T_<$ states decreases as neutron number increases for Mo isotopes, as shown in Fig. 7. This may be connected with an increase in the excitation energy E of the composite nucleus with neutron excess for Mo isotopes. The leading term in Eq. (1) can be reduced to an approximate relation for a fixed outgoing energy as follows,

$$\left[\frac{d\sigma_x}{d\epsilon}\right]_{n=3} \propto \frac{1}{KA_cE^3}\ , \tag{10}$$

where K is the K value in $|M|^2$ and A_c the mass number of the composite nucleus. Thus, we can reasonably see the trend of the decreasing $T_<$ component from Eq. (10). Contrary to this trend, however, the experimental cross sections integrated from 10 to 13 MeV have almost constant values for all Mo isotopes, as shown in Fig. 3. In previous (p,p') works,[37,38] it was shown that the collective character becomes more apparent as the mass number increases for Mo isotopes. In fact, bump structures due to overlapping of strong peaks were observed in the present (p,p') spectra corresponding to residual excitations around 2 MeV for the target nuclei, except for shell closed nuclei. Such collective excitations due to direct processes may contribute to the continuous region of excitations higher than 4 MeV. Some underestimation for ^{98}Mo and ^{100}Mo seems to be related to this contribution.

In the low proton energy region, where the contribution from multiparticle emission cannot be neglected, fairly good agreement between the calculated and experimental spectra were shown in Figs. 7 and 8. Since this component depends strongly upon the model parameters, such as level density parameter and γ-decay width, it would be necessary to adjust such parameters for better agreement with the experimental spectra.

V. SUMMARY

The measured proton spectra from 18 MeV (p,p') scattering by nuclei around $N=50$ have shown no appreciable shell and odd-even effects in the continuum region corresponding to residual excitations above 4 MeV, where the preequilibrium emissions are dominant.

These observations were reasonably interpreted through considerations of the state densities generated from two sets of single particle levels; one is based on the spherical Nilsson model and the other is based on the MUS model, in which the shell gap was introduced into the US model. The MUS model reproduced well the averaged behavior of state densities obtained from the spherical Nilsson model in the excitation region of above 4 MeV. As a result, it was confirmed that the Williams formula was a reasonable approximation in the excitation energy region higher than 4 MeV even for nuclei near the shell closure.

The measured energy spectra were compared with those calculated on the basis of the exciton model and the Hauser-Feshbach model, in which the isospin selection rule was taken into account. In the exciton model calculation, the shell-independent single particle level density was employed and the standard pairing shift of Blann *et al.*[27] was implemented in the p-h state density as a pairing correction. Good agreement between the experimental and calculated spectra was obtained in the outgoing proton energy of 3–14 MeV, regardless of rough assumptions on the isospin mixing.

It was found that preequilibrium emissions from $T_>$ states of the composite nucleus do not mainly contribute to the (p,p') spectra in the outgoing energy region higher than 10 MeV. On the other hand, the dominant $T_<$ component in the region decreased with increasing neutron number for Mo isotopes, and the (p,p') spectra were somewhat underestimated for ^{98}Mo and ^{100}Mo. The underestimation may partly be ascribed to the fact that the excitations due to direct process have been ignored in the present analysis.

The authors would like to thank members of the Nuclear Physics Laboratory of the Department of Physics, Kyushu University, for their assistance in operating the accelerator.

*Present address: Sasebo Technical College, Sasebo, Japan.
†Present address: Mitsubishi Electric Industrial Co. Ltd., Kobe, Japan.
‡Present address: Toshiba Corporation, Kawasaki, Japan.

[1]W. Scobel, M. Blann, T. T. Komoto, M. Trabandt, S. M. Grimes, L. F. Hansen, C. Wong, and B. A. Pohl, Phys. Rev. C **30**, 1480 (1984).
[2]E. Mordhorst, M. Trabandt, A. Kaminsky, H. Krause, and W. Scobel, Phys. Rev. C **34**, 103 (1986).
[3]F. C. Williams, Jr., A. Mignerey, and M. Blann, Nucl. Phys.

A207, 619 (1973).
[4]K. Albrecht and M. Blann, Phys. Rev. C **8**, 1481 (1973).
[5]S. M. Grimes, J. D. Anderson, J. W. McClure, B. A. Pohl, and C. Wong, Phys. Rev. C **7**, 343 (1973); S. M. Grimes, J. D. Anderson, J. C. Davis, and C. Wong, *ibid.* **8**, 1770 (1973); S. M. Grimes, J. D. Anderson, and C. Wong, *ibid.* **13**, 2224 (1976).
[6]M. Blann, S. M. Grimes, L. F. Hansen, T. T. Komoto, B. A. Pohl, W. Scobel, M. Trabandt, and C. Wong, Phys. Rev. C **32**, 411 (1985).
[7]I. Kumabe, Y. Mito, M. Hyakutake, N. Koori, H. Sakai, and Y. Watanabe, Phys. Rev. C **35**, 467 (1987).
[8]F. D. Becchetti, Jr. and G. W. Greenlees, Phys. Rev. **182**, 1190 (1969).
[9]F. G. Perey, Phys. Rev. **131**, 745 (1963).
[10]B. L. Cohen, G. R. Rao, C. L. Fink, J. C. van der Weerd, and J. A. Penkrot, Phys. Rev. Lett. **25**, 306 (1970).
[11]C. Kalbach-Cline, J. R. Huizenga, and H. K. Vonach, Nucl. Phys. **A222**, 405 (1974).
[12]M. Blann, Annu. Rev. Nucl. Sci. **25**, 123 (1975).
[13]A. Iwamoto and K. Harada, Phys. Rev. C **26**, 1821 (1982).
[14]C. Kalbach, Z. Phys. **A283**, 401 (1977).
[15]F. C. Williams, Jr., Nucl. Phys. **A166**, 231 (1971).
[16]E. Běták, Comput. Phys. Commun. **9**, 92 (1975).
[17]S. G. Nilsson, K. Dansk. Vidensk. Selsk. Mat.-Fys. Medd. **29**, No. 16 (1955).
[18]A. Bohr and B. R. Mottelson, *Nuclear Structure* (Benjamin, Reading, MA, 1975), Vol. II, p. 649.
[19]N. Zeldes, A. Grill, and A. Simievic, K. Dansk. Vidensk. Selsk. Mat.-Fys. Medd. **3**, No. 5 (1967).
[20]I. Kumabe and Y. Watanabe, Phys. Rev. C **36**, 543 (1987).
[21]K. Kikuchi and M. Kawai, *Nuclear Matter and Nuclear Reactions* (North-Holland, Amsterdam, 1968), Chap. 2.
[22]W. Hauser and H. Feshbach, Phys. Rev. **87**, 366 (1952).
[23]C. Kalbach, S. M. Grimes, and C. Wong, Z. Phys. A **275**, 175 (1975).
[24]S. M. Grimes, J. D. Anderson, A. K. Kerman, and C. Wong, Phys. Rev. C **5**, 85 (1972).
[25]D. Wilmore and P. E. Hodgson, Nucl. Phys. **55**, 673 (1964).
[26]G. S. Mani, M. A. Melkanoff, and I. Iori, Centre a l'Energie Atomique Report No. CEA 2379 (unpublished).
[27]M. Blann and H. K. Vonach, Phys. Rev. C **28**, 1475 (1983).
[28]C. Kalbach-Cline, Nucl. Phys. **A210**, 590 (1973).
[29]J. D. Anderson, C. Wong, and J. W. McClure, Phys. Rev. **138**, B615 (1965).
[30]J. R. Huizenga and G. Igo, Nucl. Phys. **29**, 462 (1962).
[31]D. M. Brink, Ph.D. thesis, Oxford University, 1955.
[32]P. Axel, Phys. Rev. **126**, 671 (1962).
[33]J. M. Blatt and U. F. Weisskopf, *Theoretical Nuclear Physics* (Wiley, New York, 1952), Chap. XII.
[34]A. Gilbert and A. G. W. Cameron, Can. J. Phys. **43**, 1446 (1965).
[35]*Table of Isotopes*, 7th ed., edited by C. M. Lederer and V. S. Shirley (Wiley-Interscience, New York, 1978).
[36]H. Malecky, L. B. Pikel'ner, I. M. Salamatin, and E. I. Sharapov, Yad. Fiz. **13**, 240 (1971) [Sov. J. Nucl. Phys. **13**, 133 (1971)].
[37]Y. Awaya, K. Matsuda, T. Wada, N. Nakanishi, and S. Takeda, J. Phys. Soc. Jpn. **33**, 881 (1972).
[38]S. J. Burger and G. Heymann, Nucl. Phys. **A243**, 461 (1975).